IEEE Access
Multidisciplinary | Rapid Review | Open Access Journal

Received 23 May 2024, accepted 25 July 2024, date of publication 2 August 2024, date of current version 12 August 2024.

Digital Object Identifier 10.1109/ACCESS.2024.3437373

RESEARCH ARTICLE

Time Pickoff Method Using Dual-Edge Discrimination to Mitigate Time Walk

JEONG HUN SHIN, JEONG ROK GIM, AND HANSANG LIM, (Senior Member, IEEE)
Department of Electronic Convergence Engineering, Kwangwoon University, Seoul 01897, South Korea

Corresponding author: Hansang Lim (lhs@kw.ac.kr)

This work was supported by the Basic Science Research Program through the National Research Foundation of Korea under Grant NRF-2021R1F1A1045896.

ABSTRACT Precise generation of a timing pulse at the signal is crucial for high-resolution time measurements, accomplished using a time pickoff circuit. The primary challenge in time pickoff circuits is to minimize the dependency of timing pulse generation on signal amplitude, which causes a timing error known as time walk. This study proposes a time pickoff method using dual-edge discrimination, which measures the crossing times of the signal at both its leading and trailing edges and calculates a reference time when the signal reaches its peak amplitude. The proposed time pickoff method was theoretically analyzed, demonstrating that the reference time was independent of variations in the crossing times due to the signal amplitude variations. Furthermore, the timing error caused by the charge sensitivity of the comparator used in the time pickoff circuit was reduced. The proposed time pickoff method was validated through experiments for signals with 2-ns rise and 3-ns fall times and amplitudes ranging from 18 mV to 1.8 V, resulting in a time walk of 145 ps.

INDEX TERMS Charge sensitivity, dual-edge discrimination, time-of-flight, time pickoff, time walk.

I. INTRODUCTION

Time-of-flight (TOF) refers to the time interval when a signal travels to an object and back. This measurement is extensively used for object detection and localization across various applications, including medical imaging [1], [2], particle physics [3], [4], and environmental sensing [5], [6], [7]. Measuring TOF requires a precise timing pulse when the signal returns; a time pickoff circuit is employed to generate the pulse. A precise time pickoff is essential for high-resolution object detection because the location of the object is calculated from the measured TOF. However, time pickoff circuits are prone to timing errors, known as time walk, due to their dependence on signal amplitude.

Figure 1 illustrates the two main causes of time walk for signals with identical rise and fall times but different amplitudes. Although the signals occur simultaneously, the timing pulses are generated at different times because of the varying crossing times of the threshold (left panel, Figure 1). The right panel shows that the signals cross the threshold simultaneously, but the timing pulses are generated at different times due to charge sensitivity. It implies that the propagation delay of the comparator in the time pickoff circuit varies with the input signal characteristics, such as overdrive, underdrive, and slew rate.

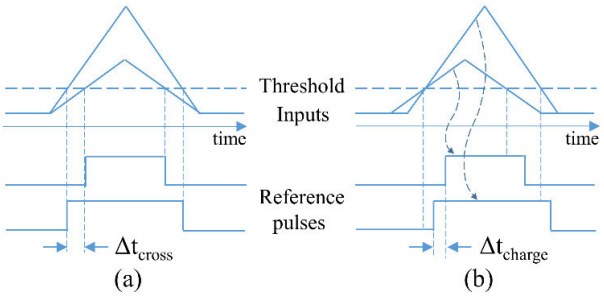

FIGURE 1. Main causes of time walk.

Three types of time pickoff circuits are widely used: leading-edge discriminators (LED), constant-fraction discriminators (CFD), and zero-crossing discriminators (ZCD).

The associate editor coordinating the review of this manuscript and approving it for publication was Wei Wei.

An LED generates a timing pulse when the signal crosses a predefined threshold level [8], [9], [10]. Such discriminator is popular due to its simple structure, ease of setup, and wide input range. However, it suffers from significant timing errors because the crossing time varies with the signal amplitude. Additional measurements of amplitude-related features, such as signal amplitude, width, and slew rate, are used to improve timing accuracy [8], [9], [10].

A CFD uses a constant fraction point on the leading edge of the input signal as the reference time, comparing an attenuated signal with a delayed input signal [11], [12], [13]. The crossing time for signals with a constant rise time remains independent of the signal amplitude, resulting in minimal timing error primarily due to charge sensitivity. However, the input range of a CFD is narrower than that of an LED because the crossing point falls outside the constant fraction of the signal if the signal is saturated.

A ZCD uses the time when the derivative of the input signal crosses zero voltage, indicating a polarity change in the signal slope, as the reference time [14], [15], [16]. This method typically differentiates the input signal to identify a zero-crossing point. The zero-crossing time remains independent of signal amplitude for inputs with a constant rise time because the signal slope changes polarity at its peak point, resulting in minimal timing errors caused only by charge sensitivity. However, the timing information at the peak is lost if the signal is saturated, reducing the input range of the ZCD compared to the LED.

Careful design of circuit parameters is essential for optimal timing performance in CFDs and ZCDs: it includes the attenuation ratio and delay amount for CFDs, while it involves selecting appropriate component values such as resistors and capacitors in the differentiator circuit, as well as the threshold level, for ZCDs. A trade-off exists between timing performance, implementation complexity, and allowable input dynamic range. Both CFD and ZCD circuits exhibit amplitude dependence of timing pulses due to charge sensitivity.

Approaches using automatic gain control (AGC) have been investigated to reduce time walks by minimizing signal amplitude variations before the comparator stage [17], [18], [19]. This method decreases the timing dependence on signal amplitude. However, AGC-based methods suffer from low count rates due to the requirement of a long internal delay and variable response times of the involved variable-gain amplifier, which limits their applicability and timing performance.

This study proposes a time-pickoff method using dual-edge discrimination to overcome existing limitations. The method used the peak point of the input signal as the reference time. It measured the crossing times of the leading and trailing edges of the input signal with a predefined threshold and calculated the reference time using both edges. This approach ensures easy setup and minimizing timing errors because the time to reach the peak point is independent of signal amplitude. When calculating the reference time, the effects of charge sensitivity on the timing-pulse generation at both edges are mitigated, further reducing the resulting timing error.

The main contributions of this study are as follows:

1) Proposing a new time pickoff method that combines leading- and trailing-edge discrimination to generate a reference time corresponding to the peak amplitude of the signal.

2) Theoretically analysing the operational principle of the proposed method, which demonstrates that the reference time is independent of variation in crossing times due to the signal amplitude, the primary cause of timing errors.

3) Reducing the effects of charge sensitivity in a comparator, a secondary cause of timing error, and facilitating easy setup by simply comparing signals at both edges with the threshold.

The remainder of this paper is organized as follows: Section II presents the operational principle of the proposed time-pickoff method. Section III describes the experiments to validate the proposed method and analyses the resulting performance. Section IV concludes the study.

II. TIME PICKOFF USING DUAL-EDGE DISCRIMINATION

The fundamental principle of the proposed time pickoff method is outlined, followed by an examination of its operational mechanisms. Subsequently, the impact on charge sensitivity is addressed.

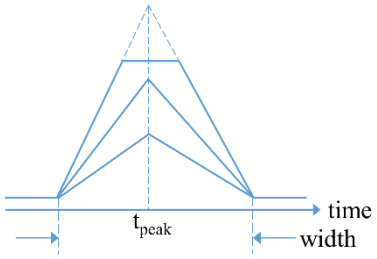

FIGURE 2. Peak time of the signals with different amplitudes.

A. BASIC CONCEPT

Consider signals with identical rise and fall times. Figure 2 shows that time (t_{peak}) at which the signals attain their peak point, referred to as the peak time, remains constant irrespective of their amplitudes. The signal profile was simplified to a straight line at the leading and trailing edges. The proposed method used the said peak time as the reference time, comparing signals at these edges against a predefined threshold and determining the crossing times. Subsequently, the peak time was estimated using two crossing times and unaffected by signal amplitude variations. Although the uppermost signal was saturated, its virtual peak time, indicated by the dashed line, coincided with that of unsaturated signals. Therefore, the proposed time pickoff method supports a wider dynamic input range than CFD or

TABLE 1. Time-related symbols.

	Ideal signal	Real signal (i = 1,2)
Crossing time of the leading/trailing edge with the threshold	t_{up} / t_{dn}	t_{upi} / t_{dni}
Time between crossing times of leading and trailing edges	t_w	t_{wi}
Time between leading/trailing edge crossing times of ideal and real signals	-	Δt_{upi} / Δt_{dni}
Time between crossing time and timing pulse generation time for real signals	-	$t_{pd(upi)}$ / $t_{pd(dni)}$

ZCD provided the signal width remains identical, even under saturation.

B. THEORETICAL ANALYSIS

Estimating peak time through leading- and trailing-edge discrimination was analysed. A general pulse-shaped signal was considered. Two signals with the same full width at half maximum (FWHM) and rise and fall times but different amplitudes are shown in Figure 3.

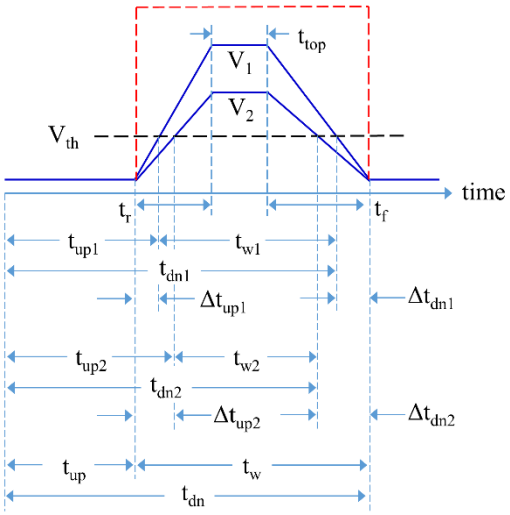

FIGURE 3. Timing diagram excluding a propagation delay.

The dashed red line illustrates the ideal pulse signal with zero transition times. The solid blue lines depict two real signals with non-zero transition times, denoted as rise time (t_r) and fall time (t_f). The peak amplitudes of these signals are denoted as V_1 and V_2, respectively. We assumed that the rise and fall times corresponded to the transition times from 0 to 100% and from 100 to 0%, respectively. The dashed black line represents the threshold level (V_{th}). Other time-related symbols are listed in Table 1.

The crossing times of real signals, t_{upi} and t_{dni} (i = 1, 2), can be ascertained from measurements, from which t_{wi} was subsequently derived. Given that rise and fall times remain fixed for real signals, the ratio t_f to t_r is a constant (k), i.e., $t_f = k \cdot t_r$. The relationship between timing information for each signal i can be expressed as follows:

$$t_{upi} = t_{up} + \Delta t_{upi} \tag{1}$$

$$t_{dni} = t_{dn} - \Delta t_{dni} \tag{2}$$

$$t_{wi} = t_{dni} - t_{upi} = t_w - \Delta t_{upi} - \Delta t_{dni} \tag{3}$$

Subsequently, the slopes of leading- and trailing-edges, Δt_{upi} and Δt_{dni}, can be determined by:

$$\frac{V_i}{t_r} = \frac{V_{th}}{\Delta t_{upi}} \rightarrow \Delta t_{upi} = \frac{V_{th}}{V_i} t_r \tag{4}$$

$$\frac{V_i}{t_f} = \frac{V_{th}}{\Delta t_{dni}} \rightarrow \Delta t_{dni} = \frac{V_{th}}{V_i} t_f = k \Delta t_{upi} \tag{5}$$

The reference time (t_{ref}) is independent of signal amplitude because it is established as a virtual peak time. Hence, t_{ref} can be expressed as follows:

$$t_{ref} = t_{up1} + \alpha t_{w1} = t_{up2} + \alpha t_{w2} = const, \tag{6}$$

where α is a constant. By substituting (1)–(3) into (6), the relationship between the second and third parts in (6) is given by

$$(1-\alpha)\Delta t_{up1} - \alpha \Delta t_{dn1} = (1-\alpha)\Delta t_{up2} - \alpha \Delta t_{dn2}. \tag{7}$$

Since $\Delta t_{dni} = k \Delta t_{upi}$ in (5), (7) can be expressed as

$$[1 - \alpha\,(1 + \mathrm{k})]\left(\Delta t_{up1} - \Delta t_{up2}\right) = 0 \tag{8}$$

Given the distinct amplitudes of two signals, i.e., $V_1 \neq V_2$, $\Delta t_{up1} \neq \Delta t_{up2}$. Therefore, to satisfy (8), the constant α should be set to be

$$\alpha = \frac{1}{1+k} \tag{9}$$

After applying (9) to (6), the reference time is expressed as:

$$t_{ref} = t_{up1} + \frac{1}{1+k} t_{w1} = t_{up1} + \frac{1}{1+k}(t_{dn1} - t_{up1}) \tag{10}$$

$$= t_{up} + \Delta t_{up1} + \frac{1}{1+k}\left[t_w - (1+k)\,\Delta t_{up1}\right]$$

$$= t_{up} + \frac{1}{1+k} t_w \tag{11}$$

It is shown that the reference time corresponds to the peak time and remains independent of signal amplitude because t_{up} and t_w represent timing parameters for an ideal signal and remain unaffected by signal amplitude. Moreover, the reference time remains valid even in signal saturation, provided that signal width remains constant.

C. EFFECTS OF THE CHARGE SENSITIVITY

In Section II-B, the propagation delay of the comparator employed for generating a timing pulse was neglected. The timing pulse was assumed to be initiated precisely when the signal crossed the threshold. However, the comparator experienced a non-negligible propagation delay, which fluctuated with amplitude-related attributes of the input signal, including overdrive, underdrive, and slew rate, owing to the charge sensitivity of the comparator. Consequently, the

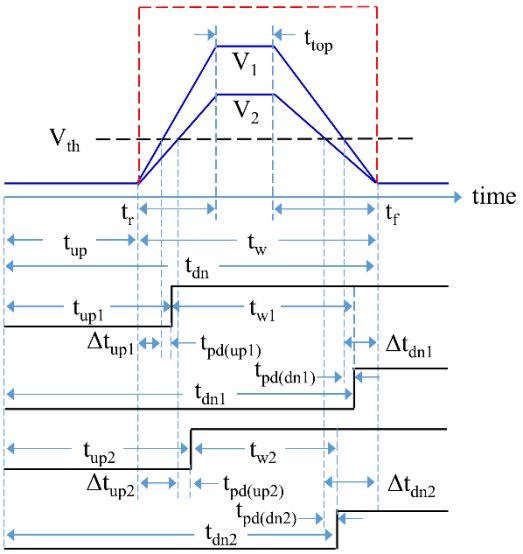

FIGURE 4. Timing diagram considering a propagation delay of a comparator.

dependence of the proposed time pickoff method on charge sensitivity was analysed.

Figure 4 illustrates the correlation between the input signals and timing pulses, considering the propagation delay of the comparator. The solid black lines represent resultant timing pulses, typically generated employing a comparator. The propagation delays, $t_{pd(upi)}$ and $t_{pd(dni)}$, from the leading and trailing edges crossing times to the initiation of the output pulse of the comparator, respectively, were considered.

The relationship between timing information can be expressed as follows:

$$t_{upi} = t_{up} + \Delta t_{upi} + t_{pd(upi)} \tag{12}$$

$$t_{dni} = t_{dn} - \Delta t_{dni} + t_{pd(dni)} \tag{13}$$

$$\begin{aligned} t_{wi} &= t_{dni} - t_{upi} \\ &= t_w - \Delta t_{upi} - \Delta t_{dni} - t_{pd(upi)} + t_{pd(dni)} \end{aligned} \tag{14}$$

The actual reference time for signal i can be derived by applying (9,12–14) to (6), as follows:

$$t_{refi} = t_{upi} + \frac{1}{1+k} t_{wi} \tag{15}$$

$$= t_{up} + \frac{1}{1+k} t_w + \frac{k}{1+k} t_{pd(upi)} + \frac{1}{1+k} t_{pd(dni)} \tag{16}$$

While the first and second terms in (16) are independent of the signal amplitude, the third and fourth terms vary due to the dependence of $t_{pd(upi)}$ and $t_{pd(dni)}$ on overdrive, underdrive, and slew rates, which fluctuate with signal amplitude.

Considering this dependency, the propagation delays $t_{pd(upi)}$ and $t_{pd(dni)}$ can be approximated as:

$$t_{pd(xi)} = t_{pd(x)} + \Delta t_{pd(xiover/under)} + \Delta t_{pd(xislew)}, \tag{17}$$

where x represents *up* or *dn*, denoting the leading or trailing edges, respectively. $t_{pd(x)}$ represents a constant corresponding to a typical propagation delay, while $\Delta t_{pd(xiover/under)}$ and $\Delta t_{pd(xislew)}$ denote variations in propagation delay due to changes in overdrive or underdrive and slew rate at the crossing point, respectively. Therefore, the variation in the reference time can be expressed as:

$$\begin{aligned} \Delta t_{refi} = &\frac{k}{1+k}\left[\Delta t_{pd(upiover)} + \Delta t_{pd(upislew)}\right] \\ &+ \frac{1}{1+k}\left[\Delta t_{pd(dniunder)} + \Delta t_{pd(dnislew)}\right] \end{aligned} \tag{18}$$

The fluctuations in timing pulse generation times at the leading and trailing edges were mitigated by $\frac{k}{1+k}$ and $\frac{1}{1+k}$, respectively. Moreover, the underdrive at the trailing edge remained consistent for all signals, with variations in the generation time of the timing pulse at the trailing edge primarily attributable to the slew rate.

III. PERFORMANCE OF THE PROPOSED TIME PICKOFF METHOD

The performance of the proposed time pickoff method using dual-edge discrimination was evaluated experimentally.

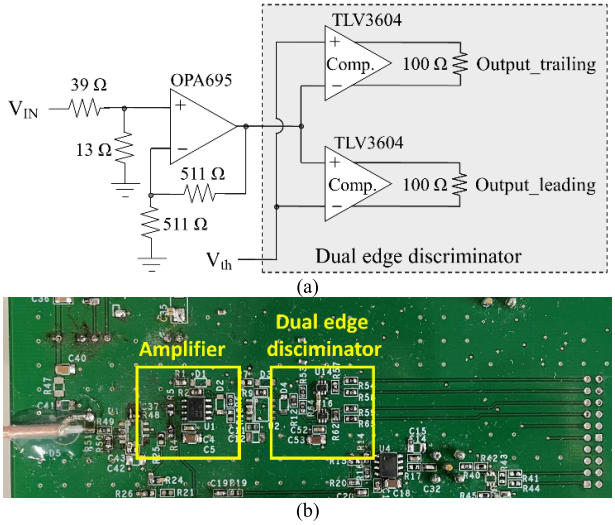

FIGURE 5. (a) Circuit diagram of the proposed time pickoff and (b) its photograph.

A. EXPERIMENTAL SETUP

Figure 5 depicts the circuit diagram employed in the experiments and the fabricated test circuit, comprising an amplifier and a dual-edge discriminator. The input signal was amplified using a current-feedback operational amplifier (OPA695, Texas Instruments) with a gain of 2. A current-feedback operational amplifier was selected owing to its high slew rate to accommodate steep rise and fall times. The amplified signal was directed to a dual-edge discriminator comprising two comparators (TLV3604, Texas Instruments), where it was compared to the predefined threshold level at both its leading and trailing edges. The threshold level was established at 20 mV, the lowest feasible value, to ensure a broad dynamic range of inputs.

Two experiments were conducted. The first experiment aimed to validate the concept of the proposed approach by measuring the crossing times at both edges of the amplifier output and calculating the reference time using (10). The second one assessed the performance of the proposed method by measuring the generation times of the comparator output at both edges of the signal and deriving the reference time from these measurements.

The amplitudes of the input signal under test ranged from 18 mV to 1.8 V. Its rise time, fall time, and width were 2 ns, 3 ns, and 4 ns, respectively. The rise and fall times corresponded to the transitions between 10% and 90% of the maximum amplitude, denoted as $t_{r(10-90)}$ and $t_{f(90-10)}$, respectively, because setting the transition time from 0% to 100% was practically unfeasible. The width represents the FWHM. The input signal was generated using a pulse generator (HP81110A, Agilent) and fed into the circuit through an SMA (subminiature version A) connector. A resistive divider was inserted between the SMA connector and amplifier because of the limited output range of the pulse generator. The outputs of the amplifier and timing pulse, i.e., the output of the comparator, were measured using a digital oscilloscope (DSO-S 104A, Keysight) with a bandwidth and sampling rate of 2.5 GHz and 20 GSa/s, respectively.

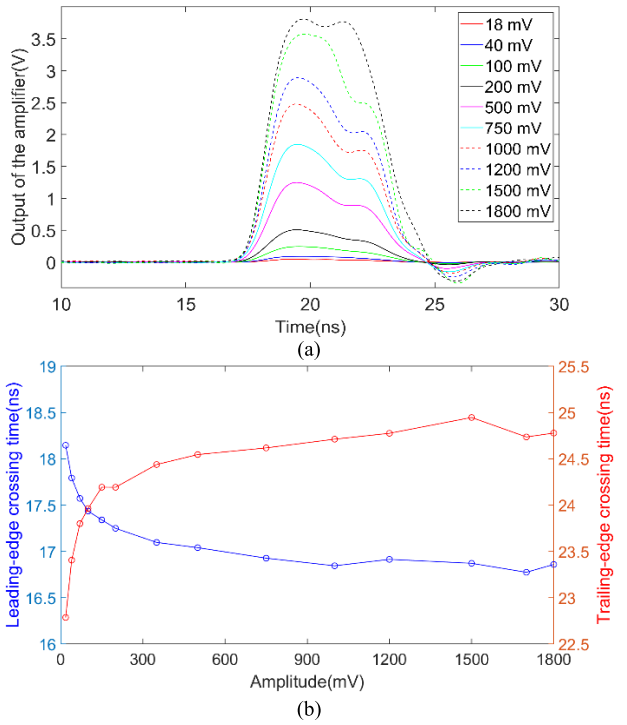

FIGURE 6. (a) Outputs of the amplifier. (b) Crossing times of the amplifier outputs at the leading and trailing edges.

B. EXPERIMENTAL RESULTS

First, the output signals of the amplifier were measured for input signals with varying amplitudes (see Figure 6(a)). One hundred measurements were conducted for each input signal at a constant amplitude. The times when the leading and trailing edges of the output signals intersected the predefined threshold (denoted as t_{upi} and t_{dni} for $i = 1$ and 2 in Figure 3) were derived from the measured results using MATLAB (see Figure 6(b)). The blue and red lines represent the averages of the crossing times at the leading and trailing edges for each amplitude, respectively.

A larger input signal crossed the threshold earlier at the leading edge, whereas a smaller one crossed earlier at the trailing edge. Therefore, the crossing time at the leading edge decreased while that at the trailing edge increased with increasing signal amplitude. The crossing times at the leading edge changed by 1.372 ns, ranging from 18.147 to 16.775 ns, which causes time walk in the LEDs. The variation in crossing times at the trailing edge was 2.160 ns, ranging between 22.287 and 24.947 ns.

Subsequently, the reference time (t_{ref}) was calculated from the crossing times of the amplifier output signals using (10), which solely considered the effects of signal amplitude on crossing time. Considering $t_{r(10-90)} = 2$ ns and $t_{f(90-10)} = 3$ ns for the input signals, k in (10) was set to 1.5, assuming a linear extension of transition times. The reference times for diverse signal amplitudes were averaged for each amplitude (see Figure 7). The variation in average reference time, i.e., the time, was 142 ps, ranging from 19.960 to 20.102 ns for a 40 dB dynamic range. The dependency of the reference time on signal amplitude was reduced by over 85% compared to the crossing time at the leading edge of the signal, affirming the validity of the proposed dual-edge discrimination-based time pickoff method.

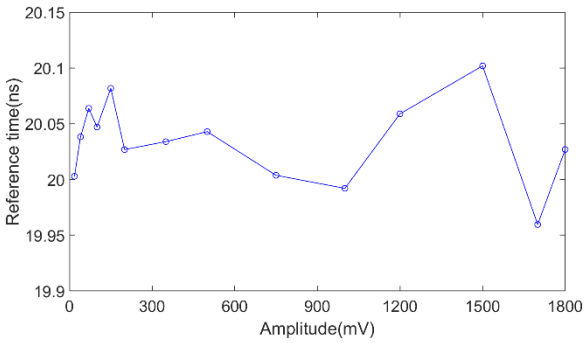

FIGURE 7. Reference times obtained from the amplifier outputs.

Second, the timing pulses at the two comparators of the dual-edge discriminator were measured for signals with varying amplitudes. Subsequently, the generation times at the leading and trailing edges (t_{upi} and t_{dni} in Figure 4) were determined from the middle level of the LVDS output swing, i.e., 1.2 V (see Figure 8). The blue and red lines represent t_{upi} and t_{dni}, respectively. As the signal amplitude ranged from 18 mV to 1.8 V, t_{upi} varied by 1.344 ns from 21.928 to 20.584 ns, and t_{dni} varied by 1.800 ns from 26.960 to 28.760 ns. The variation in t_{upi} obtained from the comparator outputs was approximately the same as in the crossing times

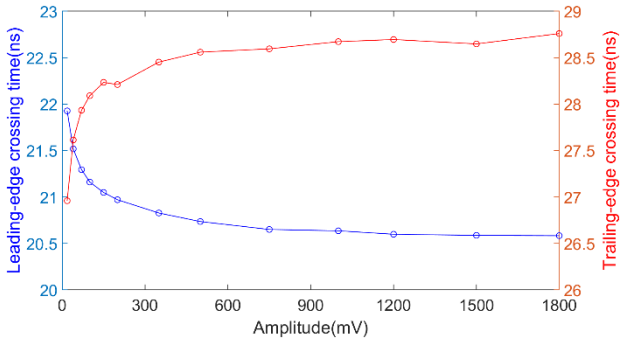

FIGURE 8. Timing pulse generation time of the comparator at the leading and trailing edges.

obtained from the amplifier outputs, while t_{dni} decreased by 359 ps.

The timing pulse at the comparator was generated after a propagation delay from when the input signal crossed the predefined threshold. The propagation delay changed with the input signal attributes, such as overdrive, underdrive, and slew rates. The propagation delays were approximately consistent at the leading edge except for signals with amplitudes of 18 mV and 1.5 V, suggesting a partial cancellation of the effects of input signal attributes on the propagation delay of the comparator. However, the propagation delays decreased at the trailing edge as the signal amplitude increased.

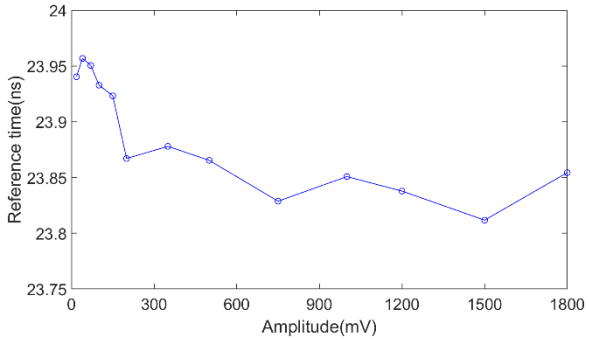

FIGURE 9. Reference times of the proposed dual-edge discrimination-based time pickoff method.

The reference times were computed from the measured timing pulses of the comparator, t_{upi} and t_{dni}, using (15). Their averages for each signal with a fixed amplitude are shown in Figure 9. These reference times encompassed the effects of signal amplitude on both the crossing time and propagation delay of the comparator and demonstrated the timing performance of the proposed dual-edge discrimination-based time pickoff method. The variation in average reference times, i.e., time walk, was 145 ps for input signals with a 40 dB dynamic range, which was reduced by approximately 90% than LEDs. It validates the efficacy of the proposed time pickoff method.

The variance in reference times derived from the timing pulse of the comparator was approximately identical to that in the crossing time obtained from the amplifier output in Figure 7. This comparison highlights that the timing error induced by the charge sensitivity of the comparator is significantly reduced using the proposed method. As described in (18), the proposed time pickoff method mitigated the impacts of overdrive, underdrive, and slew rates at the leading and trailing edges by $\frac{k}{1+k}$ or $\frac{1}{1+k}$.

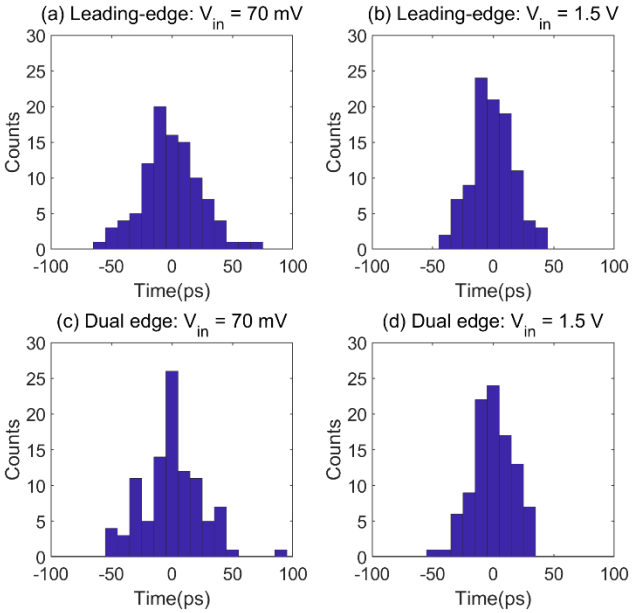

FIGURE 10. Statistical distribution of the reference time: (a) and (b) 70 mV and 1.5 V in an LED; (b) and (d) 70 mV and 1.5 V in the dual-edge discriminator.

Figure 10 compares the statistical distributions of the reference times of the proposed method with those of the leading-edge discriminators. Figures 9(a) and 9(b) depict the results for signals with amplitudes of 70 mV and 1.5 V in the LED, while Figures 9(c) and 9(d) correspond to the outcomes of the proposed method. The standard deviations for Figure 9(a)–9(d) are 23.6 ps, 17.2 ps, 24.3 ps, and 17.3 ps, respectively. The statistical distribution of the proposed time pickoff method is akin to that of the LEDs. Notably, the small input signal is more susceptible to jitter due to a lower slew rate, leading to larger deviations in the reference time for input signals with an amplitude of 70 mV than those with an amplitude of 1.5 V in both the LED and proposed time pickoff method.

IV. CONCLUSION

A time pickoff method based on dual-edge discrimination was proposed to mitigate the influence of input signal amplitude on timing pulse generation. This method estimates the peak time of the signal with fixed rise and fall times using the crossing times of the input signal at its leading and trailing edges. The peak time information remains unaffected by the signal amplitude because signals with fixed rise and fall times reach their peak amplitudes concurrently.

The proposed time pickoff method underwent theoretical analysis, and its validity was affirmed by examining the mea-

sured outputs of the amplifier. Subsequently, the performance of the proposed method was assessed using the measured timing pulses of the comparator, which encapsulated the effects of signal amplitude on both crossing times and the charge sensitivity of the comparator. These timing pulses typically become inputs of the time-to-digital converter for time measurements. Consequently, time walk, denoting the variance in the reference time, was determined to be 145 ps for input signals featuring a 2-ns rise time, 3-ns fall time, and 4-ns width, spanning a 40 dB dynamic range of amplitudes from 18 mV to 1.8 V. A comparative analysis of the results obtained from the amplifier and comparator showed a reduction in charge sensitivity (i.e., additional timing error due to the propagation delay dispersion) of the comparator, as outlined in the theoretical analysis.

Future endeavors will explore the effects of input signal characteristics, such as rise and fall times, signal width, timing performance advancements, and dynamic range expansion.

REFERENCES

[1] V. Westerwoudt, M. Conti, and L. Eriksson, "Advantages of improved time resolution for TOF PET at very low statistics," *IEEE Trans. Nucl. Sci.*, vol. 61, no. 1, pp. 126–133, Feb. 2014, doi: 10.1109/TNS.2013.2287175.

[2] H. Kim, C.-M. Kao, Y. Hua, Q. Xie, and C.-T. Chen, "Multiplexing readout for time-of-flight (TOF) PET detectors using striplines," *IEEE Trans. Radiat. Plasma Med. Sci.*, vol. 5, no. 5, pp. 662–670, Sep. 2021, doi: 10.1109/TRPMS.2021.3051364.

[3] M. Bogomilov, A. Artamonov, S. Giani, D. Kolev, J. Panman, R. Tsenov, and I. Tsukerman, "Physics performance of the barrel RPC system of the HARP experiment," *IEEE Trans. Nucl. Sci.*, vol. 54, no. 2, pp. 342–353, Apr. 2007, doi: 10.1109/TNS.2006.890323.

[4] J. Lu, L. Zhao, J. Qin, H. Xu, J. Cao, S. Liu, and Q. An, "Readout electronics prototype of TOF detectors in CEE of HIRFL," *IEEE Trans. Nucl. Sci.*, vol. 68, no. 8, pp. 1976–1983, Aug. 2021, doi: 10.1109/TNS.2021.3093544.

[5] K. Ürkmen and E. Yüce, "Design of a high-resolution multifocal LiDAR: Enabling higher resolution beyond the laser pulse rise time," *IEEE Trans. Instrum. Meas.*, vol. 72, pp. 1–6, 2023, doi: 10.1109/TIM.2023.3241051.

[6] S. Cattini, D. Cassanelli, L. D. Cecilia, L. Ferrari, and L. Rovati, "A procedure for the characterization and comparison of 3-D LiDAR systems," *IEEE Trans. Instrum. Meas.*, vol. 70, pp. 1–10, Dec. 2021, doi: 10.1109/TIM.2020.3043114.

[7] H. Seo, H. Yoon, D. Kim, J. Kim, S.-J. Kim, J.-H. Chun, and J. Choi, "Direct TOF scanning LiDAR sensor with two-step multi-event histogramming TDC and embedded interference filter," *IEEE J. Solid-State Circuits*, vol. 56, no. 4, pp. 1022–1035, Apr. 2021, doi: 10.1109/JSSC.2020.3048074.

[8] H. Lim and J. Parka, "Comparison of time corrections using charge amounts, peak values, slew rates, and signal widths in leading-edge discriminators," *Rev. Sci. Instrum.*, vol. 74, no. 6, pp. 3115–3119, Jun. 2003, doi: 10.1063/1.1571970.

[9] P. Palojarvi, T. Ruotsalainen, and J. Kostamovaara, "A 250-MHz BiCMOS receiver channel with leading edge timing discriminator for a pulsed time-of-flight laser rangefinder," *IEEE J. Solid-State Circuits*, vol. 40, no. 6, pp. 1341–1349, Jun. 2005, doi: 10.1109/JSSC.2005.848022.

[10] X. Wang, R. Ma, D. Li, H. Zheng, M. Liu, and Z. Zhu, "A low walk error analog front-end circuit with intensity compensation for direct ToF LiDAR," *IEEE Trans. Circuits Syst. I, Reg. Papers*, vol. 67, no. 12, pp. 4309–4321, Dec. 2020, doi: 10.1109/TCSI.2020.3022714.

[11] M. O. Bedwell and T. J. Paulus, "A constant fraction differential discriminator for use in fast timing coincidence systems," *IEEE Trans. Nucl. Sci.*, vol. NS-26, no. 1, pp. 422–427, Feb. 1979, doi: 10.1109/TNS.1979.4329669.

[12] M. L. Simpson, C. L. Britton, A. L. Wintenberg, and G. R. Young, "An integrated, CMOS, constant-fraction timing discriminator for multichannel detector systems," *IEEE Trans. Nucl. Sci.*, vol. 42, no. 4, pp. 762–766, Aug. 1995, doi: 10.1109/23.467795.

[13] D. M. Binkley, B. S. Puckett, B. K. Swann, J. A. Rochelle, M. S. Musrock, and M. E. Casey, "A 10-Mc/s, 0.5-μm CMOS constant-fraction discriminator having built-in pulse tail cancellation," *IEEE Trans. Nucl. Sci.*, vol. 49, no. 3, pp. 1130–1140, Jun. 2002, doi: 10.1109/TNS.2002.1039626.

[14] B. T. Turko and R. C. Smith, "A precision timing discriminator for high density detector systems," *IEEE Trans. Nucl. Sci.*, vol. 39, no. 5, pp. 1311–1315, Oct. 1992, doi: 10.1109/23.173197.

[15] M. W. Jochmann, "Development of a CMOS integrated zero-crossing discriminator using analog continuous-time division," *IEEE Trans. Nucl. Sci.*, vol. 44, no. 3, pp. 308–311, Jun. 1997, doi: 10.1109/23.603661.

[16] A. Baharmast, S. Kurtti, and J. Kostamovaara, "A wide dynamic range laser radar receiver based on input pulse-shaping techniques," *IEEE Trans. Circuits Syst. I, Reg. Papers*, vol. 67, no. 8, pp. 2566–2577, Aug. 2020, doi: 10.1109/TCSI.2020.2983834.

[17] B. Johansson, "A new solution of the finite rise time problem by means of a distributed amplifier with automatic gain control," *Nucl. Instrum. Methods*, vol. 6, pp. 201–205, Dec. 1959, doi: 10.1016/0029-554X(59)90122-3.

[18] H. Lim, "A time-pickoff method using automatic gain control to reduce time walk," *IEEE Trans. Nucl. Sci.*, vol. 58, no. 3, pp. 1196–1200, Jun. 2011, doi: 10.1109/TNS.2011.2130541.

[19] H. Lim, "Constant fraction discriminator involving automatic gain control to reduce time walk," *IEEE Trans. Nucl. Sci.*, vol. 61, no. 4, pp. 2351–2356, Aug. 2014, doi: 10.1109/TNS.2014.2339362.

JEONG HUN SHIN received the B.S. degree in electronic convergence engineering from Kwangwoon University, Seoul, South Korea, in 2023, where he is currently pursuing the M.S. degree. His research interests include sensor monitoring systems, such as pulsed LiDAR readout electronics.

JEONG ROK GIM received the B.S. degree in electronic convergence engineering from Kwangwoon University, Seoul, South Korea, in 2023, where he is currently pursuing the M.S. degree. His research interests include sensors and wide bandwidth signal conditioning circuits.

HANSANG LIM (Senior Member, IEEE) received the B.S., M.S., and Ph.D. degrees from the School of Electrical Engineering, Seoul National University, Seoul, South Korea, in 1996, 1998, and 2004, respectively. He was with the Telecommunications Research and Development Center, Samsung Electronics Company Ltd., from 2004 to 2007. He is currently a Professor with the Department of Electronic Convergence Engineering, Kwangwoon University, Seoul. His research interests include low-noise, high-speed signal-conditioning circuits, precise time measurements, electrical power distribution, in-vehicle network designs, and energy management in electrified vehicles.